Chapter 13
Characterization of Nonlinear Joint Stiffness Using Dynamic and Static Experimental Methods

Benjamin L. Martins, Caleb R. Heitkamp, and Joseph M. Jaeckels

Abstract An experimental study was conducted to characterize the nonlinear rotational stiffness of a missile fin control actuation system testbed. Dynamic testing was used to measure the acceleration response of the fin to a sine-sweep input at various force levels. The modal frequency and damping of the rotation mode were tracked as a function of applied force to determine the converged control surface rotation mode. Frequency response functions were generated in order to estimate the dynamic stiffness of the control actuation system joint. Static freeplay and rigidity data were also collected using an applied quasi-static load and measuring the resultant displacements at multiple locations around the fin. The freeplay and rigidity data were used to characterize the degree of nonlinearity in the joint stiffness with respect to applied load.

Keywords Control actuation system · Rotational stiffness · Nonlinear vibration · Freeplay testing

Nomenclature

ATA   ATA Engineering, Inc.
B&K   Brüel & Kjær
CAS   Control actuation system
CSLT Control surface linearity test
DAS   Data acquisition system
F&R   Freeplay and rigidity
FEM   Finite element model
FRF   Frequency response function
IMAT Interface between MATLAB, analysis, test
LVDT Linear variable differential transducer
MAC   Modal assurance criteria
UUT   Unit under test

13.1 Introduction

Over the course of a typical aerospace vehicle development cycle, aeroelastic stability of the vehicle must be verified. This verification has historically come in the form of conducting structural dynamics tests and then correlating a finite element model (FEM) of the vehicle to the test data. Once correlated, the FEM is used to perform flutter analysis at various points in the flight envelope. The degree to which the correlated FEM represents the structural dynamics of the vehicle is thus of critical importance [1].

In addition to global flexible modes, control surface rotation modes are also of interest to ensure aeroelastic stability and controllability of the vehicle. Standard practice is to perform a control surface linearity test (CSLT), where increasing levels of dynamic excitation are used to excite a control surface's rotation mode until a converged frequency is reached. During the model correlation process, the control surface joint stiffness is then adjusted until the rotation mode of the control surface matches the converged experimental frequency. While this approach is fundamentally sound, it is possible that the amount

---

B. L. Martins · C. R. Heitkamp (✉) · J. M. Jaeckels
ATA Engineering, Inc., San Diego, CA, USA
e-mail: caleb.heitkamp@ata-e.com

of dynamic excitation applied to the test article is insufficient to characterize the joint stiffness beyond the freeplay region of the joint.

In this chapter, a study was performed which characterizes the stiffness of a control actuation system (CAS) joint testbed representative of a joint commonly found on missile fins. Dynamic testing was done to characterize the rotational frequency of the CAS fin and the frequency response functions (FRF) used to estimate the joint stiffness. A static freeplay and rigidity (F&R) test was also performed to characterize the joint stiffness to high enough force levels to extend out of the freeplay and nonlinear region.

13.2 Test Article

In order to simulate a missile fin CAS, a solid aluminum fin and adaptor were machined and coupled with a gearbox and stepper motor. The fin was trapezoidal in shape with a tip chord length of 4.125′′, a root chord length of 10.5′′, and a span of 7.75′′. The adapter was offset 0.5′′ in the direction of the leading-edge. The aluminum adapter attached the fin to the gearbox shaft using four bolts at each component. The gearbox was of the worm gear type with a gear speed reducer ratio of 30:1. The closed loop NEMA 23 stepper motor had a holding torque of 17.7 in-lb. Both the gearbox and stepper motor were purchased off the shelf. The fin, gearbox, and motor assembly were attached to a strongback mounted on a t-slot table, as shown in the schematic in Fig. 13.1. The setup was intended to provide a very stiff boundary condition in order to isolate the rotational flexibility of the fin.

13.3 Experiments

Separate test configurations and equipment were used to measure the nonlinear rotational stiffness of the CAS interface joint using both dynamic and static testing methods. An overview of the dynamic and static test setups and results is provided in the following subsections.

13.3.1 Dynamic Testing

Dynamic testing consisted of attaching an electrodynamic shaker to the fin to excite the structure while measuring the response at various locations using eight accelerometers. The shaker was attached to the trailing-edge root of the fin with accelerometers distributed about the fin. Fig. 13.2 provides an image of the test setup used for dynamic testing. An MB Dynamics Modal 110 shaker was chosen to excite the UUT, and PCB 352A21 teardrop accelerometers were selected for measuring the out-of-plane response. The excitation and response locations were chosen so as to best characterize the rigid

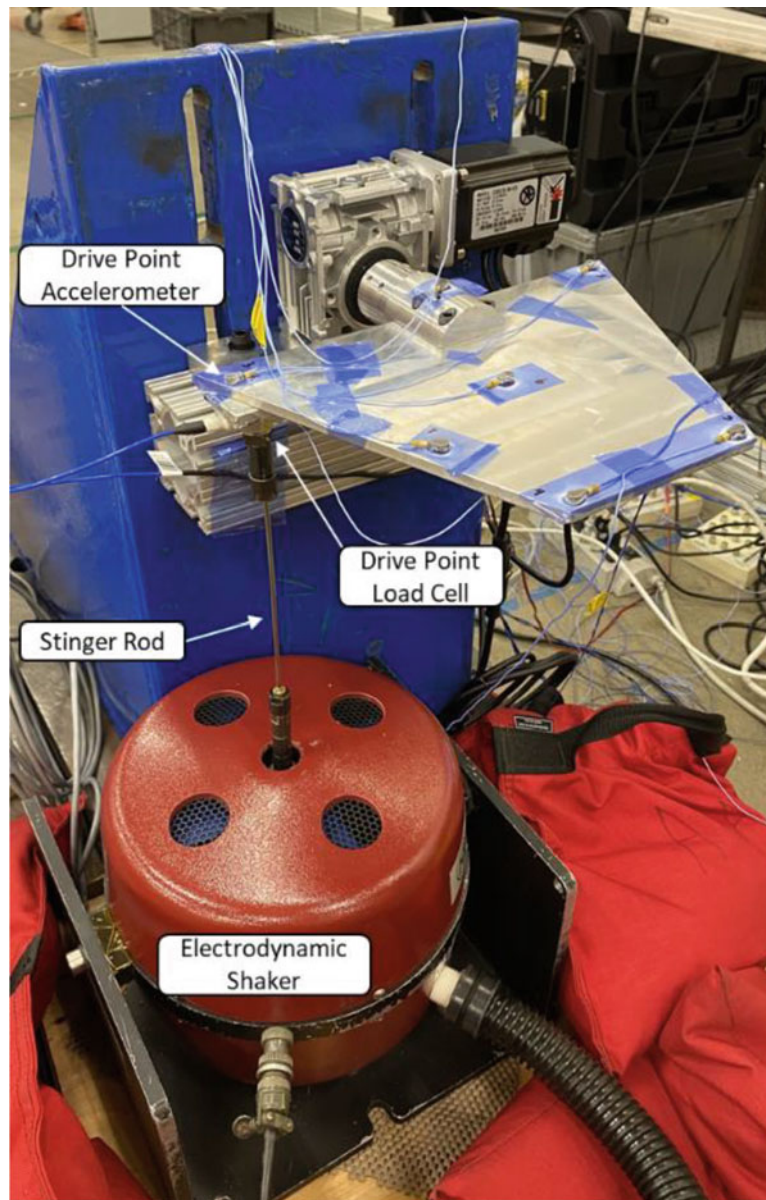**Fig. 13.1** Schematic of the unit under test (UUT) and overall test setup
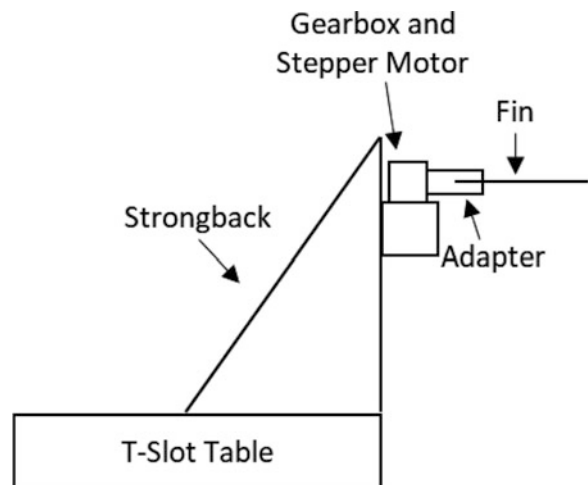
Fig. 13.2 Dynamic test setup

Table 13.1 Dynamic testing instrumentation used

Transducer	Model	Nominal sensitivity
Load cell	PCB 208C03	10 mV/lb
Accelerometer	PCB 352A21	10 mV/g
Shaker	MB Dynamics Modal 110	N/A

body rotation mode of the fin about the CAS hub. A load cell was placed at the shaker–fin interface to measure the applied dynamic force. A PCB 208C03 load cell with nominal sensitivity of 10 mV/lb. was used for the study. Table 13.1 lists the instrumentation used for the dynamic tests.

Sine sweeps were conducted over a range of up to 140 Hz to 5 Hz, while time-history data were recorded on a B&K LAN-XI data acquisition system (DAS). The time-history information of the load cell, accelerometers, and reference voltage was used to compute the FRF of the fin at various excitation force levels. The nonlinearity of the CAS interface joint proved problematic when computing the FRF via the typical "H_1" response acceleration over reference force FRF. It is thought that the out-of-band modes coupling with the modes over the excited frequency range caused poor coherence and, in turn,
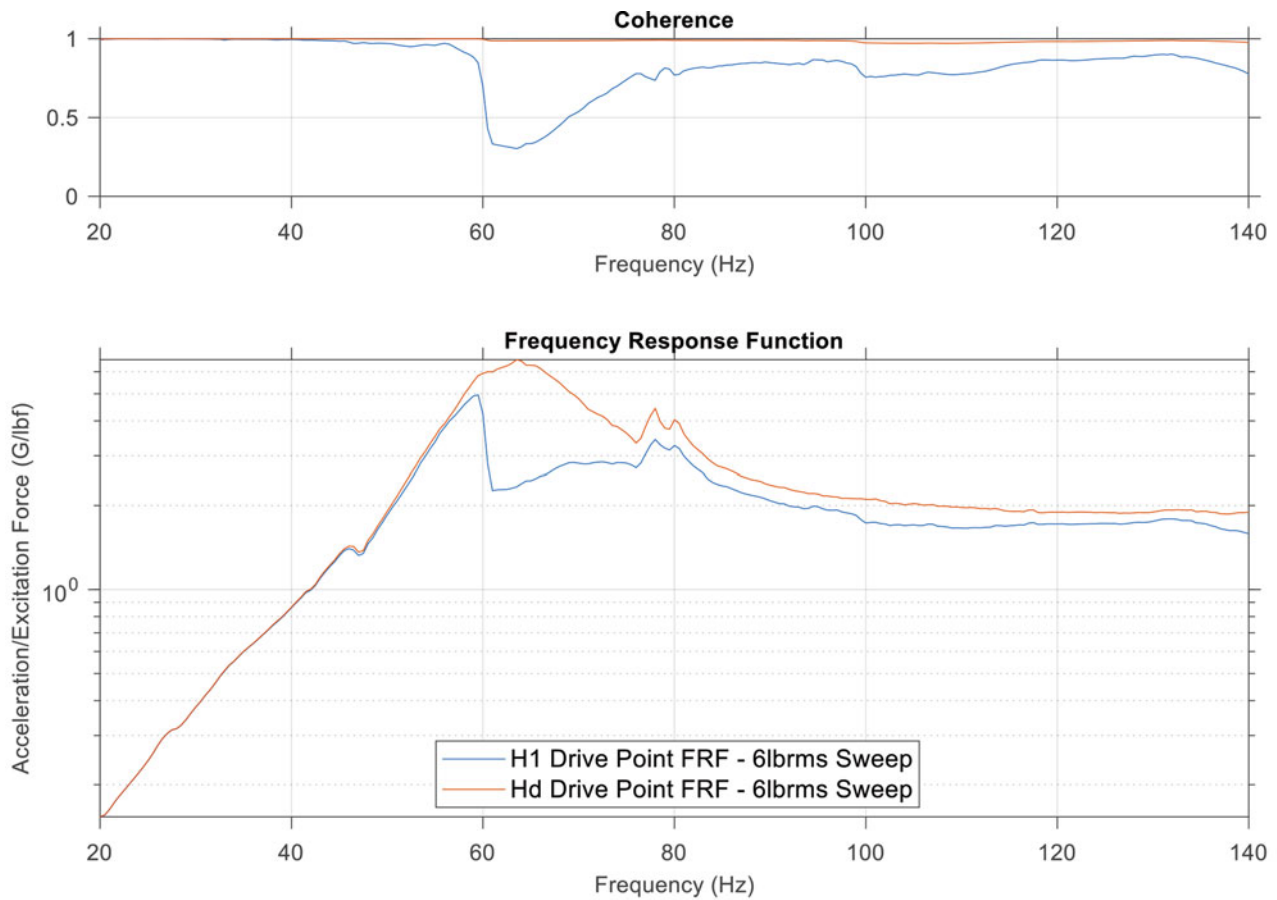
Fig. 13.3 FRF magnitude and coherence of the same data run computed using the H1 and Hd methods

unreliable FRF. To filter the out-of-band modes, the singular value decomposition method to estimate FRF [2] was used. A comparison between the H_1 and singular value decomposition FRF (H_d) is provided in Fig. 13.3.

In order to estimate the rotational dynamic stiffness of the system, the translational time-history data was converted to angular data using the geometry of the fin. The force time-history was multiplied by the chordwise distance from the CAS hinge axis to get the applied torque in units of lb-in. Likewise, the vertical acceleration time-history of the hinge axis accelerometer was subtracted from the leading-edge accelerometer location before small angle theory was applied to estimate the angular acceleration time-history of the fin. The H_d FRF of the angular acceleration relative to the applied torque was then calculated using the shaker amplifier unit voltage signal as the FRF basis. Using the input reference voltage as the basis projects the FRF onto the frequency domain encompassed by the reference voltage frequency band and filters the out-of-band modes from the acceleration response.

The locations on the fin where the excitation signal was applied and response measurements made for computation of the dynamic stiffness are shown in Fig. 13.4. Several additional accelerometers were distributed on the fin to allow for estimation of the rotational mode shape. Using the accelerometer along the root opposite, the applied load allows for a better estimate of the fin's rotation since the point is out of the load path and undergoing strain-free displacement. Likewise, subtracting the hinge vertical acceleration from the leading-edge root accelerometer accounts for any vertical rigid body deformation caused by freeplay in the CAS interface joint.

With the H_d angular acceleration FRF calculated, double integration of the FRF was conducted in the frequency domain to generate the angular displacement over applied torque FRF. For a single degree of freedom system, the low-frequency portion of the FRF corresponds to the flexibility line of the system (i.e., the inverse of the stiffness). The value of the flexibility line was computed as the average of the first 5 Hz of each respective signal. The rotation over torque FRF for each of the eight runs conducted is shown in Fig. 13.5. The calculated dynamic stiffness is listed in Table 13.2. It is important to note that the lower frequency band of the sweeps was changed between runs so as to minimize excessive shaker wear due to high amplitude, low frequency excitation force far away from the mode. The low-frequency portion of the FRF contains the most
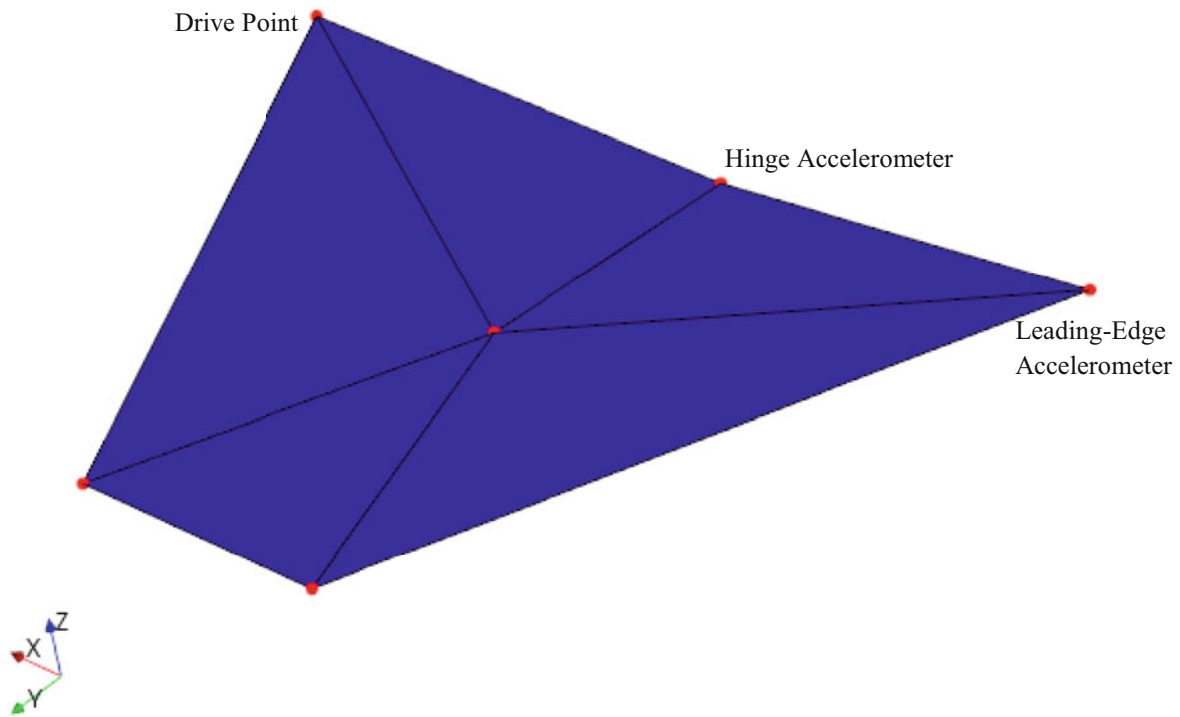
Fig. 13.4 Test display model generated for the test article showing the drive point and response locations used

accurate information related to the dynamic stiffness of the rigid body rotation, and as such, not having information at much lower frequencies than measured was a hindrance to obtaining accurate dynamic stiffness estimations, as observed by the large variation in stiffness seen in Table 13.2. This variation was particularly noticeable when the estimation range increased from 20–25 Hz to 50–55 Hz. It is thought that having FRF data down to a few Hz would result in more consistent and higher dynamic stiffness values.

The final study conducted with the dynamic test data was tracking of the frequency and damping convergence for increasing force levels. This type of study is commonly done on aircraft control surfaces and is known as CSLT. CSLT, typically, concludes when the frequency of the mode is no longer shifting relative to the applied input force level. To compute the frequency (and damping) as a function of force, the modal frequency of the rotation mode at each force level tested was estimated using the SDOFit toolkit in ATA's IMAT software. SDOFit provides the frequency and damping estimate for a single DOF system using an FRF. The mode shape was verified by animating the extracted shape at all six response locations (neglecting the drive point acceleration response) on the test display model. In this case, the drive point accelerance FRF were used to estimate the modal parameters of the rotation mode for each force level tested. Figure 13.6 shows the extracted rotation mode shape plotted on the test display model of the fin for the 2 lbrms run. The wireframe object in Fig. 13.6 is the undeformed fin, whereas the solid fin shows the displacement mode shape at the rotational resonant frequency.

The modal assurance criteria (MAC) matrix was computed for all extracted shapes to verify that the same shape was characterized for each force level. Small differences in the MAC are expected for the nonlinear system; however, the shape similarity is clearly observed in Fig. 13.7. Inspection of the mode shapes indicate that at lower force levels, the shape appears to be a pure rotation, whereas test shapes 4–8 at higher input force levels show a bending component near the load application location. This explains the difference observed in the MAC matrix, where test shapes 1–3 are very similar as are test shapes 4–8.

Once the frequency of the mode was estimated at each force level, the Fourier transform of the force time-history was used to determine the applied force level at the frequency. Table 13.3 provides the tabular data of the frequency and damping for the rotation mode at various force levels. Figure 13.8 provides a graphical representation of the same data, which indicates that the modal frequency has indeed reached convergence at the highest force level tested. This converged frequency is what is typically used as the target frequency for posttest model correlation.
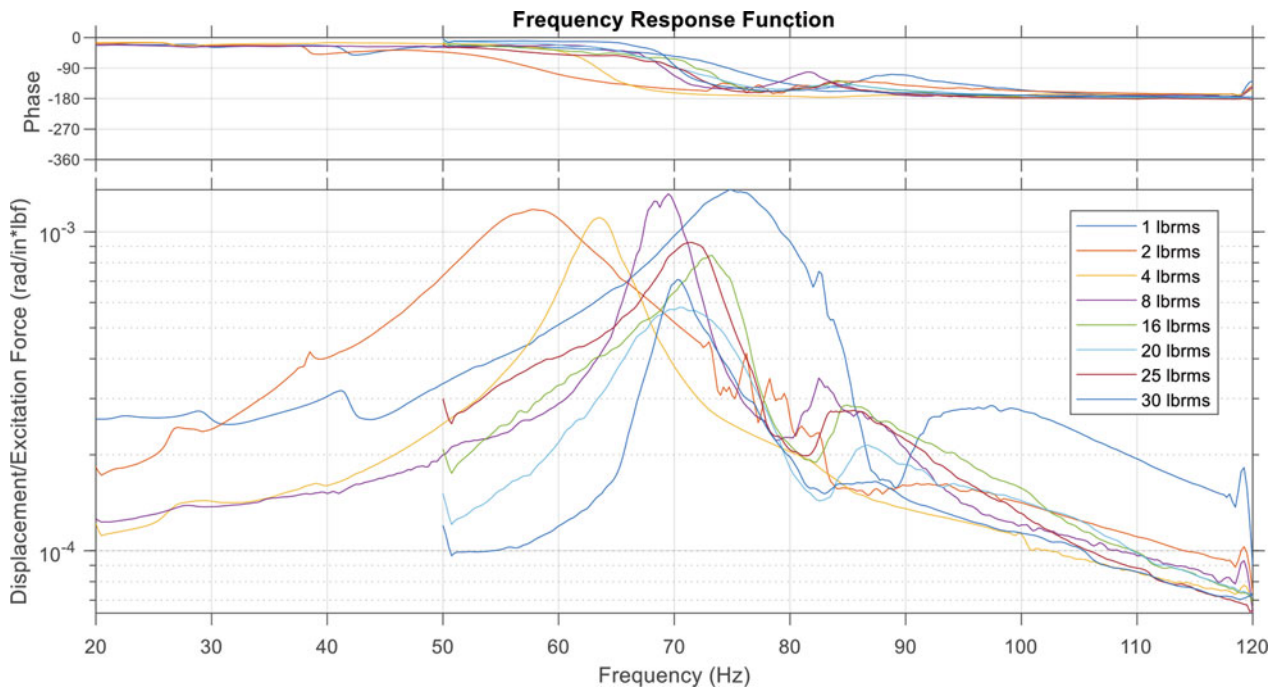
Fig. 13.5 FRF overlay for the eight nominal force levels tested

Table 13.2 Dynamic stiffness values estimated from the angular displacement FRF curves

Nominal force level (lbrms @ 120 Hz)	Rotational frequency (Hz)	Actual force at frequency (lbrms)	Rotational stiffness (in-lb/deg)	Frequency range of estimate
1	75.50	0.74	66.70	20–25 Hz
2	57.89	1.32	94.94	20–25 Hz
4	63.63	2.38	150.34	20–25 Hz
8	69.34	3.32	138.76	20–25 Hz
16	73.71	4.18	84.18	50-55 Hz
20	70.94	7.78	127.49	50–55 Hz
25	71.78	3.82	58.64	50–55 Hz
30	70.48	10.01	175.27	50–55 Hz

13.3.2 Static Testing

F&R testing was conducted on the UUT to statically characterize the stiffness of the CAS interface joint. In order to obtain F&R results, both load and displacement measurements are required to calculate the applied moment and rotation angle. A load cell was used to measure the applied load, and linear variable differential transformers (LVDTs) were used to measure the corresponding displacements of the fin. The distances from the load cell and LVDTs to the hinge line of the fin (in line with the gearbox output shaft) were used to convert load and displacement to moment and rotation angle, as was done for the dynamic tests. Transducer information and distance measurements are listed in Table 13.4. The LVDTs were mounted on an isolated assembly using tripods, and the LVDT rod ends were positioned orthogonal to the fin surface. An HBM SoMat eDAQ was used as the DAS to record the load and displacement at 200 Hz.

The load cell was positioned in series between the fin clamp and a screw-jack motor, which applied the load in a controlled manner. A ball joint was also placed in series between the load cell and the screw-jack motor to allow for purely orthogonal load inputs to the fin and to remove any potential applied moments. The motor was operated using the DAS and an ATA-developed controller specifically for F&R testing. Using the motor and controller allowed for smooth load application, consistent cycle times, and the ability to hit target hinge moments. The F&R test setup is shown in Fig. 13.9.

All displacement and load time-history data were recorded simultaneously. The test was conducted by applying five cycles of loading and unloading to the fin in both directions (positive – load cell tension and negative – load cell compression). After recording the measured data, the bending displacement (measured at LVDT 4 on the rotation hinge line) was subtracted
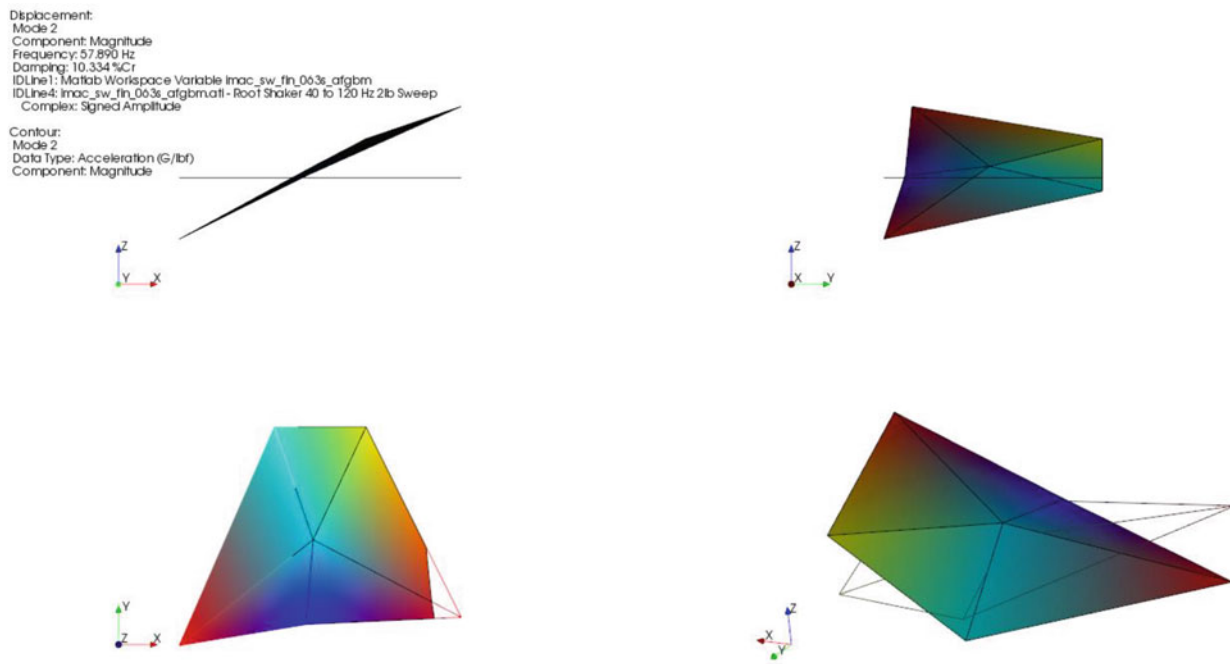
Fig. 13.6 Mode shape plot for the extracted rotation mode plotted on the test display model

Test Self MAC Table

Test Shapes

			1	2	3	4	5	6	7	8
MACtt	**Test Shapes**		75.50	57.89	63.63	69.34	73.71	70.93	71.78	70.48
100	1	75.50	100	97	98	83	90	96	89	93
95	2	57.89	97	100	100	73	78	87	78	84
90	3	63.63	98	100	100	78	82	89	82	88
85	4	69.34	83	73	78	100	97	91	98	97
80	5	73.71	90	78	82	97	100	98	100	99
75	6	70.93	96	87	89	91	98	100	97	98
70	7	71.78	89	78	82	98	100	97	100	99
65	8	70.48	93	84	88	97	99	98	99	100

Fig. 13.7 MAC of the rotation modes extracted for the various force level tested

Table 13.3 Frequency and damping of rotation modes as a function of applied force level

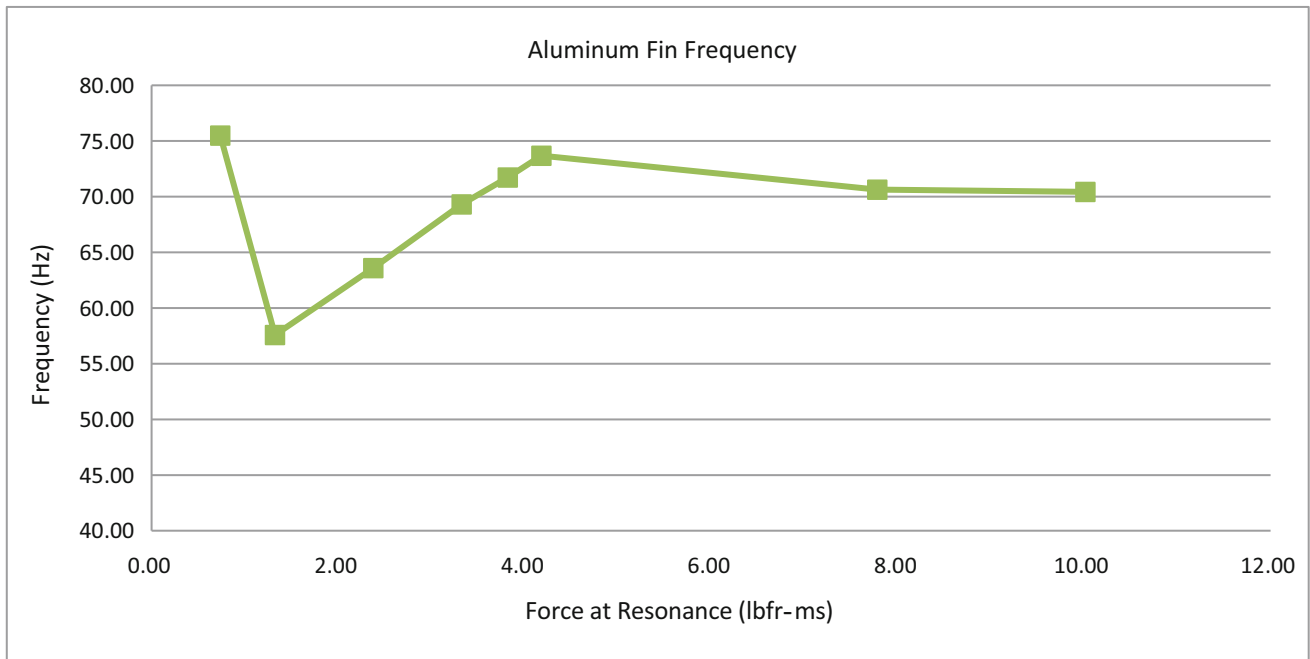| Nominal Set Force at 120 Hz (lbf-rms)	Force at Frequency (lbf-rms)	Frequency (Hz)	Damping (%Cr)	Force %Diff	Frequency %Diff
1	0.74	75.50	6.62		
2	1.32	57.58	10.33	79.6%	−23.7%
4	2.38	63.58	3.84	79.6%	10.4%
8	3.32	69.31	2.89	39.9%	9.0%
25	3.82	71.72	4.08	14.9%	3.5%
16	4.18	73.67	3.50	9.4%	2.7%
20	7.78	70.64	9.07	86.2%	−4.1%
30	10.01	70.44	3.24	28.7%	−0.3%

Fig. 13.8 Frequency of the rotation mode plotted as a function of applied force at the modal frequency

Table 13.4 List of the transducers used for the static testing

Transducer	Distance from Hinge Line (inch)	Model	Nominal sensitivity
Load cell	4.75	Interface 1500ASL-300	10 mV/lb
LVDT 1	4.25	Omega LD620-25	5000 mV/in
LVDT 2	4.50	Omega LD620-25	5000 mV/in
LVDT 3	2.00	Omega LD620-25	5000 mV/in
LVDT 4	0.00	Omega LD620-25	5000 mV/in

from the other LVDT locations to remove any bending of the test setup from the rotation displacement measurements. The displacement and load values were, respectively, converted into angular deflection (using the relative displacement between LVDT 1 and LVDT 3) and hinge moment. The moment-versus-rotation time-history plot for all cycles is shown in Fig. 13.10, and the hysteresis overlay for the three cycles used in the results is shown in Fig. 13.11. These plots show that the measurements were repeatable across cycles. A linear regression was performed on the upper and lower loading regions for each cycle in order to compute F&R values in accordance to JSSG-2006 [3] standards, as shown in Fig. 13.12. Figure 13.13 shows the linear fits and F&R results for cycle 3. The results for cycles 3, 4, and 5 are summarized in Table 13.5.

Table 13.5 shows consistent results across the three cycles used in the computation. The shaded region near the tips of the positive and negative loading cycles indicate the region from which the rigidity (stiffness) was estimated. These regions were chosen as they are responding linearly, as indicated by the dashed lines in Fig. 13.13. The consistency between cycles and also between positive and negative loading provides high confidence in the static stiffness estimates.
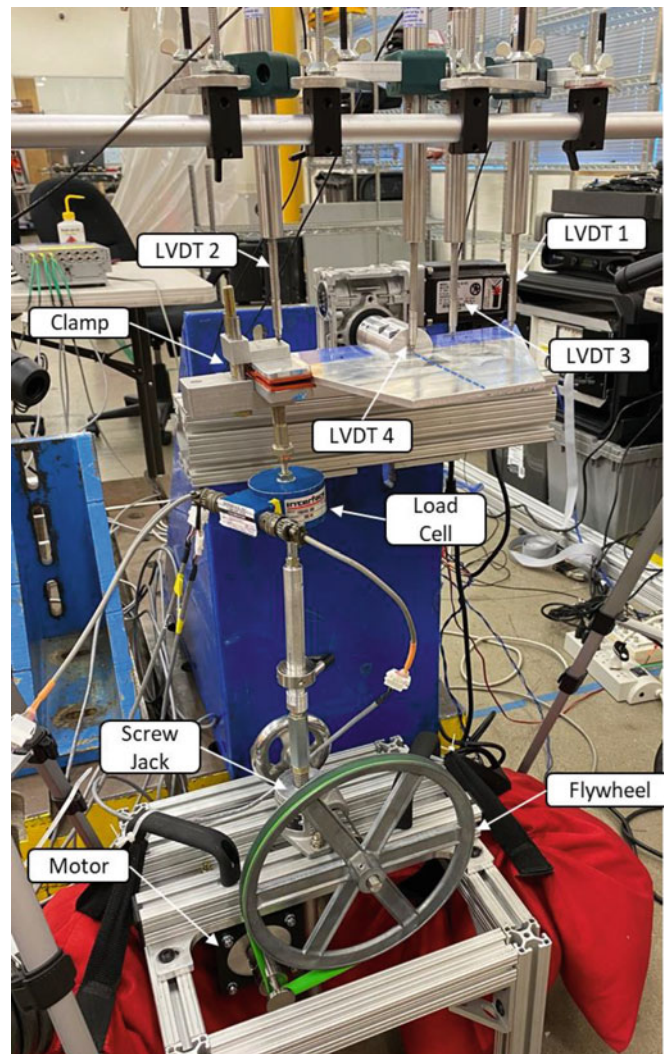
Fig. 13.9 F&R test setup

13.4 Conclusion

Static and dynamic testing was conducted on a missile fin CAS testbed to characterize the stiffness of the CAS interface joint. During dynamic testing, the rotational frequency of the fin was found to converge with respect to applied force at the modal frequency. This converged frequency was 70.5 Hz, with an estimated hinge stiffness of 175.27 in-lb/deg. at 10 lbrms. The stiffness estimates from the dynamic testing captured the general trend of increasing stiffness with increasing applied force level; however, a lack of low frequency information jeopardizes the accuracy of the stiffness estimates. It is recommended that if dynamic stiffness estimates from the FRF are desired, data are taken as low in frequency as practicable.
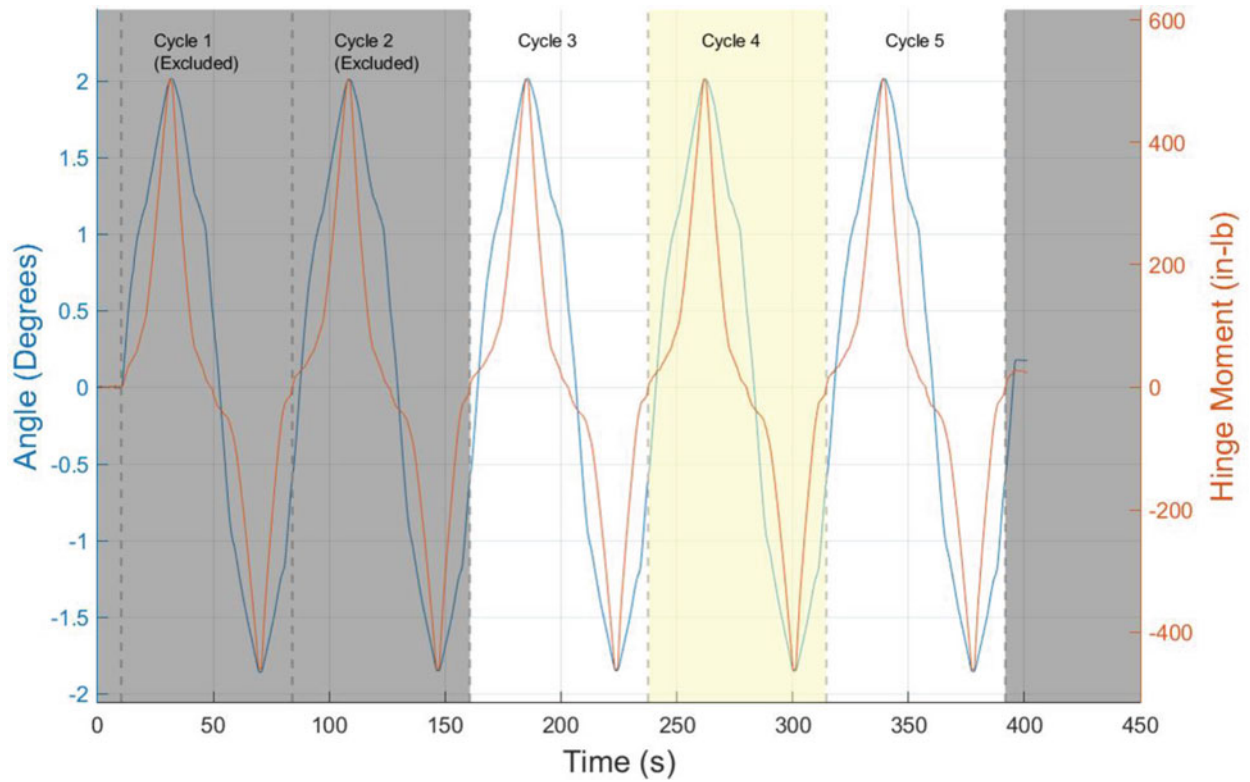
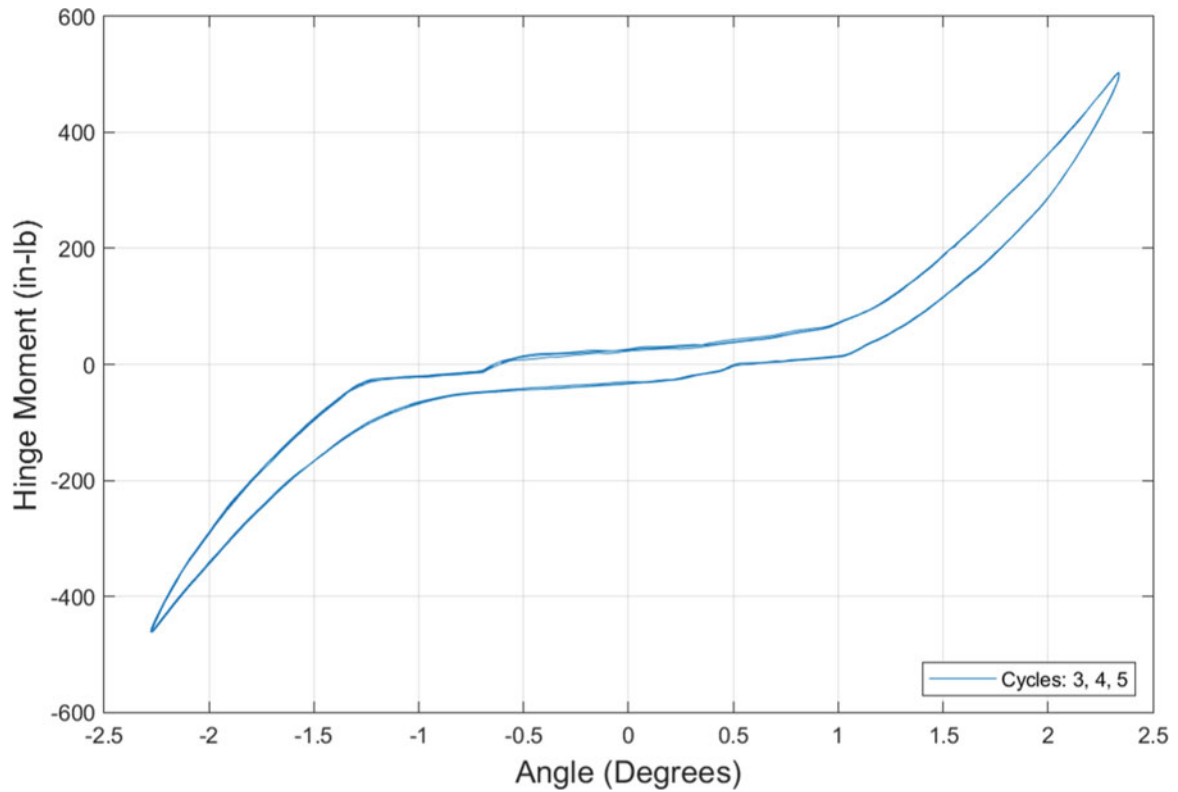**Fig. 13.10** Hinge moment and angle time-history
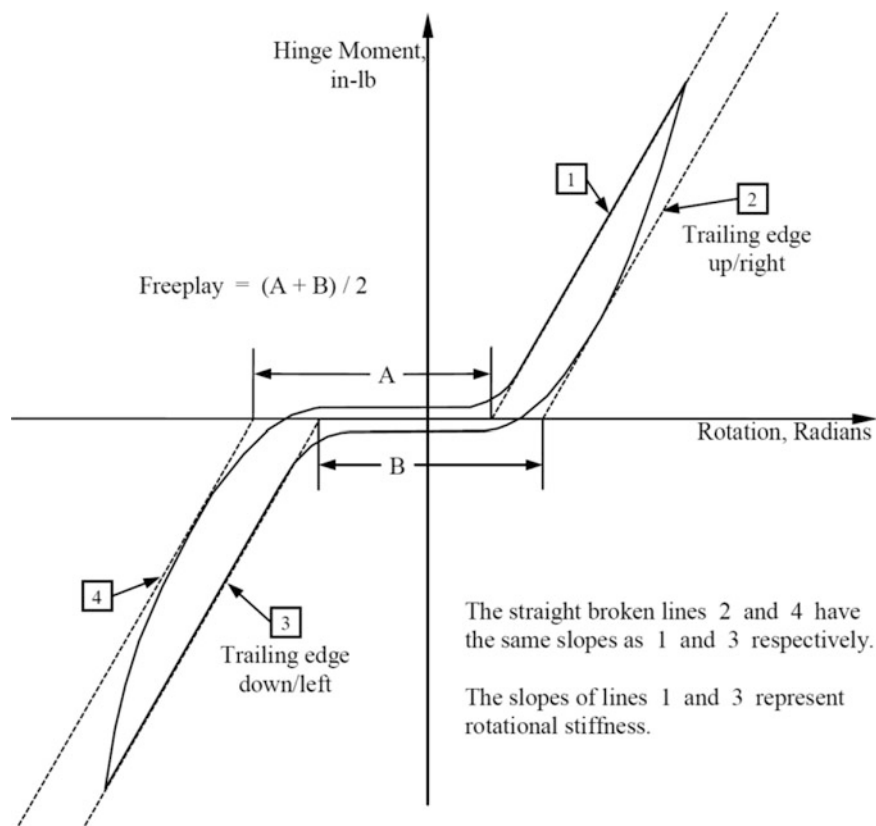

Fig. 13.11 Hysteresis overlay of cycles 3, 4, and 5

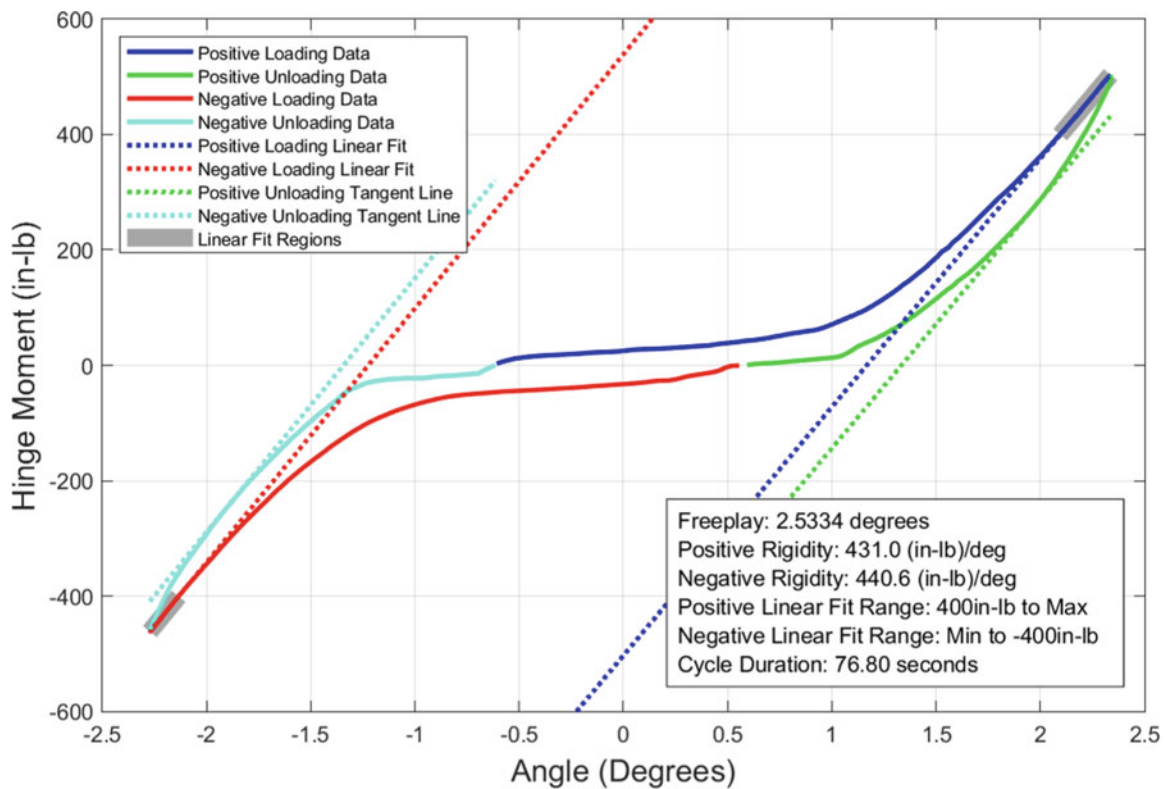**Fig. 13.12** Calculations per JSSG-2006 for freeplay and rigidity

Fig. 13.13 Hinge moment versus angle for cycle 3

Table 13.5 F&R results

Cycle	Freeplay (degrees)	Positive rigidity (in-lb/deg)	Negative rigidity (in-lb/deg)	Cycle duration (sec)	Lower bound (in-lbf)	Upper bound (in-lbf)
3	2.53	431.00	440.62	76.80	−400	400
4	2.56	440.57	442.46	76.40		
5	2.59	436.99	465.26	77.00		
Average	*2.56*	*436.19*	*449.45*	*76.73*		

The static tests revealed the hinge stiffness to be highly nonlinear at low force levels, with the stiffness not reaching a linear profile until approximately 350 in-lb of applied torque. The stiffness of the hinge at these higher force levels was estimated to be 430–440 in-lb/deg., 2.5 times higher than the hinge stiffness recovered from the dynamic tests. These results suggest that the standard practice of performing CSLT and using the converged frequency value for model correlation and flutter analysis may discount the linear CAS interface joint stiffness.

References

1. Waszak, M.R., Buttrill, C.S., Schmidt, D.K.: Modeling and Model Simplification of Aeroelastic Vehicles: An Overview. NASA Technical Memorandum (1992)
2. Napolitano, K.: Using Singular Value Decomposition to Estimate Frequency Response Functions. In: Proceedings, 34th International Modal Analysis Conference (2016)
3. JSSG-2006: DOD Joint Service Specification Guide: Aircraft Structures (1998)